# The Elastic Modulus and Fracture of Boron Carbide

G. W. HOLLENBERG* and G. WALTHER

Hanford Engineering Development Laboratory, Richland, Washington 99352

**Young's modulus at room temperature and the fracture surface energy, up to 1200°C, were determined for boron carbide specimens with 0 to 15% porosity. Sonic modulus measurements indicated that the Young's modulus decreased as porosity increased in a manner characteristic of the cylindrical pore model. The fracture surface energy appeared to be independent of porosity but was inversely related to temperature. Fractography supported the low values of fracture surface energy that were obtained.**

## I. Introduction

BORON CARBIDE is sometimes used for its mechanical or tribological properties (for instance, armor) and in other applications because of its nuclear characteristics (neutron absorber). Although not a structural load-bearing member in the latter case, the physical integrity of boron carbide in high thermal stress fields[1] is still of interest. To provide a better basis on which to evaluate the performance of boron carbide as an absorber material, elastic modulus and fracture data were obtained on boron carbide specimens with porosity levels of 0 to 15%. In addition, fracture data were obtained on 8% porosity material from 25° to 1200°C.

Many workers have characterized the moduli of boron carbide in the course of materials development efforts but Liebling[2] was the first to systematically examine the effect of porosity on the Young's modulus of boron carbide at room temperature. He measured 27 samples from 0 to 8% porosity and provided linear, quadratic, and exponential fits of the data. Hollenberg[1] presented data on boron carbide with 1 and 8% porosity from room temperature to 2000°C. These data were then fitted to the porosity-dependent expression suggested by Hasselman,[3] with a quadratic temperature dependence. Agreement between these investigations, within their limited porosity range, was good.

Primarily, strength measurements, rather than fracture mechanics measurements, have been made on boron carbide. Rice[4] reviewed the available strength data on hot-pressed boron carbide and noted that the strength was roughly inversely proportional to the square root of grain size. Dutta[5] measured the strength of experimental and commercial grades of boron carbide between room temperature and 1400°C. Room-temperature average strengths were 276 to 413 MPa. Most of these materials retained their strength up to 1400°C, but the strength of one was reduced to <69 MPa at 1400°C.

Mecholsky *et al.*[6] measured both strength and fracture toughness for hot-pressed boron carbide by using the double cantilever beam technique with a blunt saw cut for a notch. A fracture-surface energy of 15 J/m$^2$ was then used to correlate observed flaw sizes with strength values (150 to 450 MPa).

## II. Material

Boron carbide typical of that used in neutron-absorber applications was desired. Hence, the plates were hot-pressed from boron carbide powder similar to that used to fabricate absorber pellets for Fast Flux Test Facility* control-rod subassemblies. The B-to-C ratio was 3.9. The largest metallic impurity concentrations were 150 ppm Fe and 160 ppm Ti. The plates (6 by 2.5 by 0.3 cm) were cut such that crack propagation would occur in the plane normal to the hot-pressing direction. Boron carbide pellets in absorber pins have been specified to contain 6 to 10% porosity. All specimens tested at other than 500°C were within this density range. At 500°C, a temperature encountered in typical reactor operation, specimen porosity was 0 to 15%. Post-test measurements of material cut from the region near the crack tip revealed that small internal porosity variations (±1.5%) existed in the higher-porosity samples. From 0 to 15% porosity, the grain size also varied. The hot-pressing parameters that favored high density (i.e. higher temperatures, longer times, etc.) also enhanced grain growth. Samples with <8% porosity possessed average grain sizes of 2 to 7 $\mu$m, whereas samples with >8% porosity exhibited grain sizes of <2.6 $\mu$m.

## III. Experimental Procedure

Sonic moduli were measured at room temperature on the same 6.35 by 2.54 by 0.317-cm plates which were subsequently used for fracture testing. Measurement of the resonance frequencies followed an established ASTM procedure[7] and was precalibrated against a National Bureau of Standards specimen.[8] A Poisson's ratio of 0.14, as suggested by Liebling,[2] was assumed for obtaining Young's modulus.

For fracture-energy testing, the double-torsion technique was selected because the specimens could be machined from the hard material, controlled precracks could be generated, and precrack length measurements were not required. The double-torsion specimen is loaded by two upper and two lower load points at one end, such that a bending moment is applied along the central region where the crack is expected to propagate. The specimens were preloaded at a low displacement rate (0.005 mm/min) until a "pop in" was observed. A pop in or decrease in the load was used to infer that crack growth had occurred. Then, the displacement rate was increased to 0.5 mm/min and loading continued until almost instantaneous crack propagation severed the specimen.

The maximum load was used to compute the critical stress intensity factor[9]:

$$K_{IC} = PW_n[3(1+\nu)/Wt^3d_n]^{1/2} \quad (1)$$

where $W$ is the sample width, $P$ the applied load, $t$ the sample thickness, $d_n$ the groove thickness, $W_n = 9.525$ mm, and $\nu$ = Poisson's ratio. The measured sonic modulus value for each individual specimen was used in the $K_{IC}$ computation. Fracture surface energy, $\gamma_f$, for each specimen was then computed:

$$\gamma_f = [K_{IC}^2(1-\nu^2)]/2E \quad (2)$$

For tests above room temperature, moduli were adjusted using an expression for temperature dependence.[2]

To control the direction of crack growth, a channel was machined down the central region. A diamond-saw cut was made (Fig. 1) so that the crack would be propagating in a region of nearly constant $K_I$. Two sets of tests were conducted at room temperature, one with the groove down (configuration 1) and another with it up (configuration 2) as suggested by Pletka *et al.*[10] Configuration 1 did not provide valid, stable precracks; the grooved side was "leading" the crack as it propagated and, consequently, stress concentrations at the corners caused the crack to deviate to one side. In configuration 2, however, stress concentrations on the leading crack surface were avoided by having the groove up and, hence, the cracks propagated near the center of the groove.

Configuration 2 yielded more stable precracks during pop in. Of

Presented at the 81st Annual Meeting, The American Ceramic Society, Cincinnati, Ohio, April 30, 1979 (Fracture Mechanics Symposium No. 11-SII-79). Received October 9, 1979; revised copy received February 1, 1980.

Supported by the U.S. Department of Energy under Contract No. EY-76-C-142170.

*Member, the American Ceramic Society.

*Richland, Wash.

the tests at room temperature, 67% were successfully precracked; the others went to complete fracture during precracking. Samples with pop in were removed and, with the aid of die penetrant, precracks 2 to 8 mm long were observed. After complete fracture, microscopic inspection could not correlate any features with the point of pop in crack arrest. Fracture surface energies for those samples which went immediately to failure during precracking did not vary significantly (14%) from the results on precracked samples. It was decided that samples without pop in would be included in the data analysis. A crack propagating directly from a blunt saw cut could produce a positive bias, but the observed agreement supports the concept that machining flaws at the root of saw cuts can provide sharp precracks. Samples in which crack propagation did not follow the center groove were considered invalid.

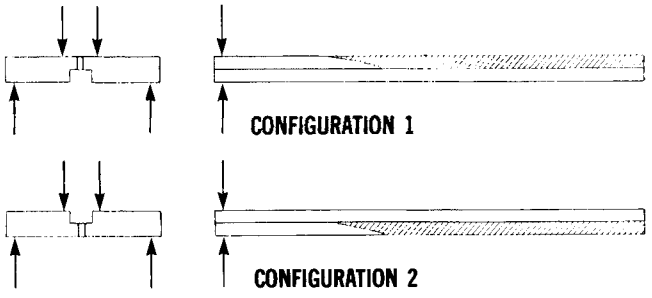


**Fig. 1.** Two loading configurations for the double-torsion technique.

Tests were conducted at 500°, 800°, and 1200°C in a flowing Ar gas atmosphere. The loading fixture during high-temperature testing was made of SiC* and SiC-$Si_3N_4$ refractory† and was contained within a split shell resistance-heated furnace. Samples were in the hot zone for 20 min prior to testing.

## IV. Modulus Results

Figure 2 shows individual modulus measurements as a function of porosity. A linear regression analysis of the data provided the following expression, the form of which was suggested by Hasselman and Fulrath[11]

$$E = 460[(1-P)/(1+2.999P)] \text{ GPa} \quad (3)$$

with a variance of 20 GPa for the 43 samples that were tested. The data of Hollenberg[1] at room temperature with only 1 and 8% porosity agree with the data from this investigation. The results of Liebling[2] appear to exhibit an increasing rate of decrease at higher porosity levels, but he obtained only three scattered data points at >5% porosity.

Figure 3 compares the modulus results with theoretical predictions derived from the rule of mixtures and from a method suggested

*KT, Carborundum Co., Niagara Falls, N.Y.
†Refrax 20, Carborundum Co.

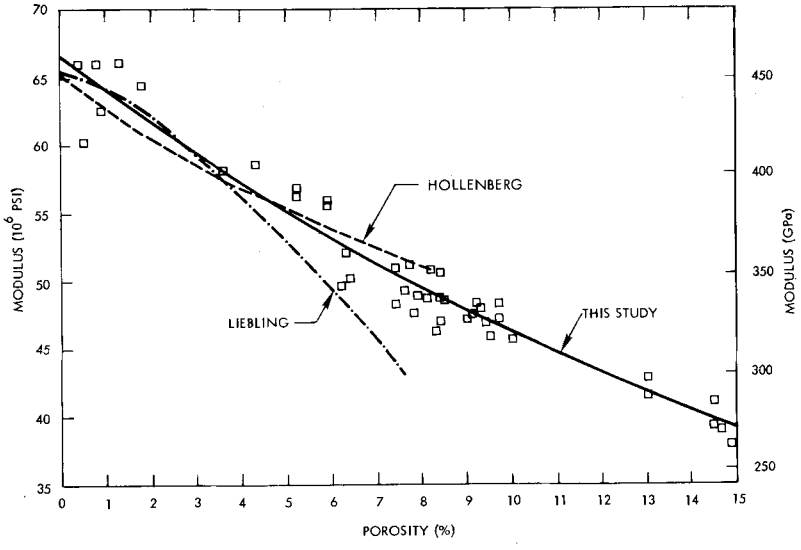


**Fig. 2.** Effect of porosity on the modulus of boron carbide at room temperature.

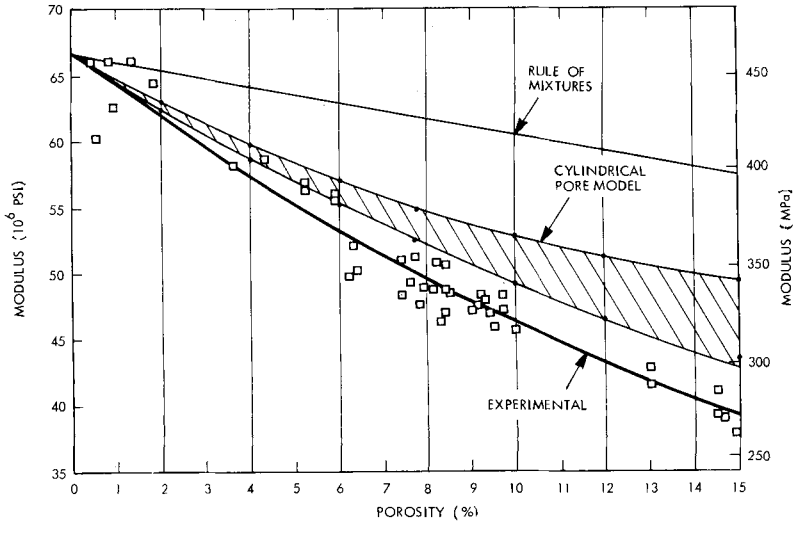


**Fig. 3.** Comparison of experimentally determined modulus values with a theoretical prediction based on the cylindrical pore model of Ref. 12.

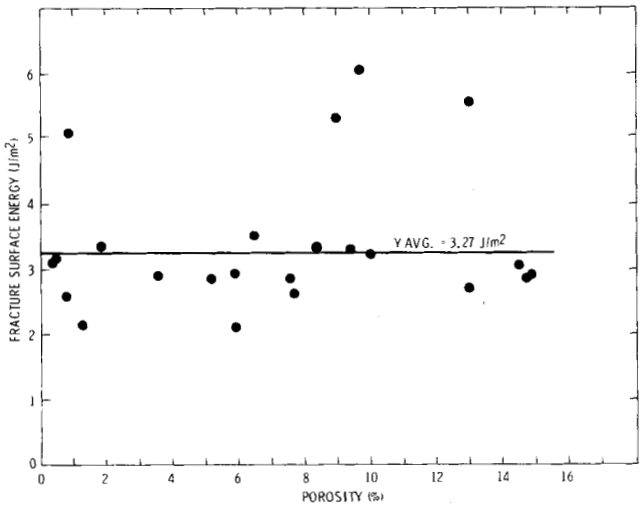


**Fig. 4.** Fracture surface energy at 500°C for boron carbide with 0 to 15% porosity.

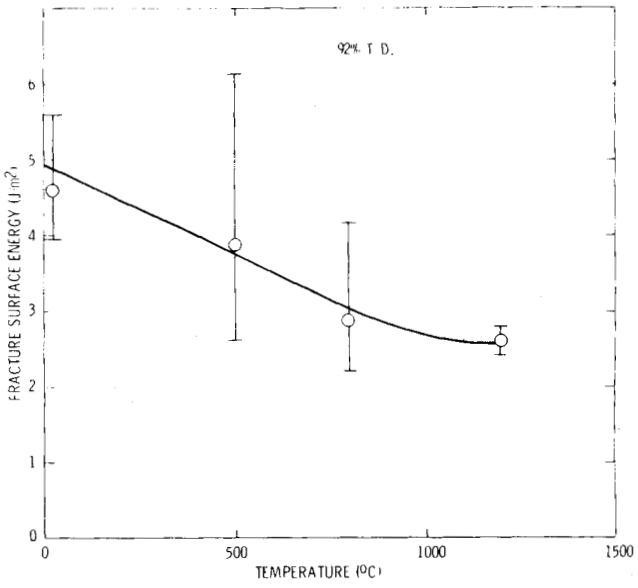


**Fig. 5.** Fracture surface energy of boron carbide with 8±2% porosity from 25° to 1200°C.

by Hashin and Rosen.[12] They analyzed a composite material which was made up of homogeneously distributed cylindrical figures in a solid matrix. Because of the complicated mathematics, Hashin and Rosen did not actually solve for the modulus, but rather obtained expressions which can be used to compute its upper and lower bounds. In these calculations the modulus values of the cylindrical fibers (pores) were assumed to equal zero and the matrix was assumed to be theoretically dense boron carbide.

In Fig. 3, the experimental modulus values are much less than the simple rule of mixtures might predict, a situation paralleling other porous ceramic systems.[11] The rule of mixtures represents an exaggerated model of the stress state in a porous material, basically, a reduction in the cross-sectional area. The model of Hashin and Rosen[12] is more representative of the complex stress state present in a porous ceramic. Figure 3 shows that the predictions for the cylindrical pore model are slightly greater than the experimental measurements. Hashin's spherical pore model[13] did not correlate with the data as well as the cylindrical pore model. In hot-pressed bodies of >5% porosity, part of the porosity can be considered cylindrical. At higher porosities the pores tend to be interconnected (open porosity) rather than isolated (closed porosity) and, hence, it is logical that the cylindrical pore model would best model the experimental results.

## V. Fracture Energy Results

Figure 4 shows the fracture surface energy, $\gamma_f$, measurements at 500°C on boron carbide containing 0 to 15% porosity. Much of the data is near the average fracture surface energy of 3.27 J/m² and there appears to be no significant effect of porosity on $\gamma_f$. Four specimens possessed significantly higher $\gamma_f$ values but no microstructural, density, or material differences could be identified. No deviations in the measurement technique were noted. The statistical variation in $\gamma_f$ does not appear excessive in comparison to that of other experimenters.[14]

The effect of temperature on $\gamma_f$ of boron carbide with 8±2% porosity is presented in Fig. 5. The data at 500°C were obtained from the results shown in Fig. 4. At each of the other temperatures, seven specimens were tested; however, at 1200°C only three tests were considered valid. The $\gamma_f$ of boron carbide with 8% porosity is ≈4.5 J/m² at room temperature but decreases to ≈2.5 J/m² at 1200°C. The critical stress intensity factor varies from ≈1.77 MPa $\sqrt{m}$ at 25° to 1.31 at 1200°C. The error bars in Fig. 5 represent the distribution of data taken at each temperature.

## VI. Fracture Energy Discussion

The $\gamma_f$ values for boron carbide in Fig. 5, obtained at room temperature, are low compared to the single data point obtained by Mecholsky *et al.* (15 J/m²).[6] In fracture testing, potential errors and invalid tests normally result in computed $\gamma_f$ values which are greater than they should be. Hence, blunt notches, misalignment of specimens, etc., that may have existed in this investigation, would increase the fracture surface rather than decrease it. Material differences exist between the two investigations.

The $\gamma_f$ values for many polycrystalline ceramics are >5 J/m². Dense $Al_2O_3$ exhibits fracture energies of 20 to 50 J/m² (Refs. 15 and 16); SiC possesses values of 14.7 to 45 J/m².[17] These values are almost an order of magnitude greater than their thermodynamic free surface energy, $\gamma_s$. In contrast, $\gamma_f$ for boron carbide in Figs. 4 and 5 approaches $\gamma_s$ for the carbides (1 to 3 J/m²).[18,19] The excess energy over and above $\gamma_s$ that is observed in $\gamma_f$ has been attributed to energy sinks associated with the fracturing process. Hasselman *et al.*[20] suggested some components for this excess energy:

$$\gamma_f = K\gamma_s + \gamma_p + \gamma_{an} + \gamma_{el} \quad (4)$$

where $K$ is the surface roughness factor and $\gamma_p$, $\gamma_{an}$, and $\gamma_{el}$ are energies expended by plastic flow, viscous flow, and the nonrecoverable elastic strain, respectively.

Since $\gamma_f$ in Figs. 4 and 5 is near anticipated values for $\gamma_s$, it follows that $\gamma_p$, $\gamma_{an}$, and $\gamma_{el}$ are very small for boron carbide. The coefficient $K$ in Eq. (4) is influenced by the tortuosity of the fracture path. Scanning electron microscopy revealed almost featureless fracture surfaces for all the boron carbide tested at 500°C. Second-phase particles or porosity can have two effects on the value of $K$ in Eq. (4). First, the porosity can cause crack branching and deflection which will increase $K$ and $\gamma_f$.[21–23] The smooth transgranular failures are in agreement, with no dependence of $\gamma_f$ on porosity and a value of $K$ near unity. A second possible influence of porosity is that $\gamma_f$ can be reduced in high-porosity materials by the effective reduction of the cross-sectional solid area. Evans and Tappin[24] observed such a decrease in $\gamma_f$ with $Al_2O_3$ from 5 to 50% porosity. The 15% change in porosity in this investigation does not constitute a major decrease in the cross-sectional solid area. Certainly, the more complex influence of grain size on $\gamma_f$ could negate any porosity effect.

In some ceramic systems, e.g. $UO_2$[14] and SiC,[25] $\gamma_f$ increases with temperature, since the $\gamma_p$ and $\gamma_{an}$ terms in Eq. (4) are increased as dislocation motion and diffusion are activated at these temperatures. But in Fig. 5, $\gamma_f$ is actually highest at room temperature. Plastic deformation does not appear to be a major factor in boron carbide. Other properties, such as the modulus[2] and plasticity,[5] in this same temperature range also imply that plastic deformation is not promi-

nent. Hence, the fact that the fracture surface energy does not increase at these high temperatures appeared to be consistent with these other properties. The apparent, small decrease in $\gamma_f$ at high temperatures is not readily explained on a theoretical basis, although the unknown temperature dependence of the $\gamma_s$ could certainly account for such a change.

## VII. Conclusion

The room temperature sonic modulus of boron carbide decreased as porosity increased in a manner anticipated from a cylindrical pore model. The fracture surface energy at 500°C was independent of porosity and was greater at room temperature (4.5 J/m²).

## References


[1]G. W. Hollenberg, "Thermally Induced Stresses and Fractures in Boron Carbide Pellets," *Am. Ceram. Soc. Bull.*, **59** [5] 538–41, 548 (1980).

[2]R. S. Liebling, "Effect of Low Porosity on the Elastic Properties of Boron Carbide," *Mater. Res. Bull.*, **2** [11] 1035–39 (1967).

[3]D. P. H. Hasselman, "On the Porosity Dependence of the Elastic Moduli of Polycrystalline Refractory Materials," *J. Am. Ceram. Soc.*, **45** [9] 452–53 (1962).

[4]R. W. Rice, "Strength/Grain Size Effects in Ceramics," *Proc. Br. Ceram. Soc.*, **1972**, No. 20, pp. 205–57.

[5]S. K. Dutta, "Boron Carbide: A Critical Study on Fabrication, Microstructure and Strength"; for abstract see *Am. Ceram. Soc. Bull.*, **54** [4] 398 (1975).

[6]J. J. Mecholsky, Jr., S. W. Freiman, and R. W. Rice, "Fracture Surface Analysis of Ceramics," *J. Mater. Sci.*, **11** [7] 1310–19 (1976).

[7]S. Spinner and W. E. Tefft, "A Method for Determining Mechanical Resonance Frequencies and for Calculating Elastic Moduli from These Frequencies," *Proc. Am. Soc. Test. Mater.*, **61**, 1221–38 (1961).

[8]R. W. Dickson and J. B. Wachtman, Jr., "An Alumina Standard Reference Material for Resonance Frequency and Dynamic Moduli Measurements: I," *J. Res. Natl. Bur. Stand., Sect. A*, **75A** [3] 155–62 (1971).

[9]A. G. Evans; pp. 17–48 in Fracture Mechanics of Ceramics, Vol. I. Edited by R. C. Bradt, D. P. H. Hasselman, and F. F. Lange. Plenum, New York, 1974.

[10]J. Pletka, E. R. Fuller, Jr., and B. G. Koepke, "An Evaluation of Double Torsion Testing"; in Symposium on Fracture Mechanics, Blacksburg, Va., June 12–14, 1978; to be published.

[11]D. P. H. Hasselman and R. M. Fulrath; pp. 343–78 in Ceramic Microstructures. Edited by R. M. Fulrath and J. A. Pask. Wiley & Sons, New York, 1968.

[12]Z. Hashin and B. W. Rosen, "The Elastic Moduli of Fiber-Reinforced Materials," *J. Appl. Mech.*, **31** [2] 223–32 (1964).

[13]Z. Hashin, "The Elastic Moduli of Heterogeneous Materials," *ibid.*, **29** [1] 143–50 (1962).

[14]A. G. Evans and R. W. Davidge, "The Strength and Fracture of Stoichiometric Polycrystalline $UO_2$," *J. Nucl. Mater.*, **33** [3] 249–60 (1969).

[15]R. W. Davidge; pp. 447–68 in Fracture Mechanics of Ceramics, Vol. 2. Edited by R. C. Bradt, D. P. H. Hasselman, and F. F. Lange. Plenum, New York, 1974.

[16]S. W. Freiman, K. R. McKinney, and H. L. Smith; pp. 672–74 in Ref. 15.

[17]J. A. Coppola and R. C. Bradt, "Measurement of Fracture Surface Energy of SiC," *J. Am. Ceram. Soc.*, **55** [9] 455–60 (1972).

[18]D. T. Livey and P. Murray, "Surface Energies of Solid Oxides and Carbides," *ibid.*, **39** [11] 363–72 (1956).

[19]R. H. Bruce; pp. 359–67 in Science of Ceramics, Vol. 2. Edited by G. H. Stewart. Academic Press, New York, 1965.

[20]D. P. H. Hasselman, J. A. Coppola, D. A. Krohn, and R. C. Bradt, "Nonrecoverable Elastic Energy and Crack Propagation in Brittle Materials," *Mater. Res. Bull.*, **7** [8] 769–72 (1972).

[21]R. G. Hoagland, C. W. Marschall, A. R. Rosenfield, G. W. Hollenberg, and R. Ruh, "Microstructural Factors Influencing Fracture Toughness of Hafnium Titanate," *Mater. Sci. Eng.*, **15** [1] 51–62 (1974).

[22]N. Claussen, "Fracture Toughness of $Al_2O_3$ with an Unstabilized $ZrO_2$ Dispersed Phase," *J. Am. Ceram. Soc.*, **59** [1–2] 49–51 (1976).

[23]C. Cm. Wu, S. W. Freiman, R. W. Rice, and J. J. Mecholsky, "Microstructural Aspects of Crack Propagation in Ceramics," *J. Mater. Sci.*, **13** [12] 2659–70 (1978).

[24]A. G. Evans and G. Tappin, "Effects of Microstructure on the Stress to Propagate Inherent Flaws," *Proc. Br. Ceram. Soc.*, **1972**, No. 20, pp. 275–97.

[25]J. L. Henshall, D. J. Rowcliffe, and J. W. Edington, "Fracture Toughness of Single-Crystal Silicon Carbide," *J. Am. Ceram. Soc.*, **60** [7–8] 373–75 (1977).


# Chemical Diffusion in Polycrystalline $Al_2O_3$


**H. A. WANG*,* and F. A. KRÖGER***

Department of Materials Science, University of Southern California, University Park, Los Angeles, California 90007



**Chemical diffusion in polycrystalline $\alpha$-$Al_2O_3$ doped with Ti or Fe was studied through the movement of a color front on oxidation of reduced samples. The diffusion is faster in polycrystalline than in single-crystal material. The oxygen pressure dependence of the rate of diffusion indicates that neutral interstitial oxygen is the major mobile species at the grain boundaries. A theory is presented which accounts for the data and explains the difference in the rates of oxidation and reduction and their dependence on oxygen pressure. Grain boundaries with precipitates of $FeAl_2O_4$ or $TiAl_2O_5$ appear to transport oxygen faster than clean boundaries.**


## I. Introduction

TRANSITION elements in $Al_2O_3$ color the sample in a manner depending on their valencies. For example: $Ti^{3+}$ (pink),[1] $Ti^{4+}$ (white), $Fe^{3+}$ (yellow), $Fe^{2+}$ (blue),[2] $Ni^{2+}$ (green),[3] $Ni^{3+}$ (yellow),[1] $Co^{2+}$ (light pink),[3,4] $Co^{3+}$ (green),[1] $V^{3+}$ (green),[1] $V^{2+}$ or $V^{4+}$ (white),[1] $Mn^{3+}$ (pink),[1] $Cu^{2+}$ (blue/green), etc.

Absorption bands responsible for these colors appear or disappear on oxidation or reduction. Titanium-doped $Al_2O_3$ is pink when the sample is annealed in a reducing atmosphere, but the color is not found in an oxidized sample in which $Ti^{3+}$ is oxidized to $Ti^{4+}$. These color centers can therefore be used as indicators of the state of oxidation of the sample if the major doping element is known. Jones *et al.*[5] used this behavior to measure the chemical diffusion coefficient involved in changing the stoichiometry of $Al_2O_3$ doped with Ti. Oxidation involves either the movement of oxygen into the sample or of aluminum out of the sample. In single crystals, $D_O \ll D_{Al}$ and the change involves migration of Al. If the migration involves charged defects ($V_{Al}'''$), it must be accompanied by migration of electronic defects (ambipolar diffusion). It has in fact been shown that, in $Al_2O_3$:Ti,[6] migration of electrons limits the rate of the oxidation-reduction processes.

Oishi and Kingery[7] showed that in polycrystalline $Al_2O_3$ (grain size 20 to 30 $\mu$m) the oxygen self-diffusion coefficient $(D_O)_{poly} >> D_O$ and not much smaller than $D_{Al}$ (which is the same for polycrystalline material and single crystals). Thus, in polycrystalline material oxidation-reduction could involve migration of either Al or O (depending on grain size), with ambipolar bulk diffusion of Al by $V_{Al}'''$ or $Al_i'''$ and $h^{\cdot}$ or $e'$ for grains >20 $\mu$m,[8] but grain-boundary diffusion of oxygen for grains <20 $\mu$m. Since oxidation-reduction also affects the electrical conductivity, this


Received October 29, 1979; revised copy received March 11, 1980.

Supported by the U.S. Department of Energy under Contract No. EY-76-03-0113, Project Agreement 27.


*Member, the American Ceramic Society.

*Now with Signetics Corp., Sunnyvale, California 94086.